Korean J. Chem. Eng., 34(10), 2686-2702 (2017)
DOI: 10.1007/s11814-017-0166-2

pISSN: 0256-1115
eISSN: 1975-7220

Prediction of critical temperature, critical pressure and acentric factor of some ionic liquids using Patel-Teja equation of state based on genetic algorithm

Hamidreza Bagheri*, and Ali Mohebbi*,†**

*Department of Chemical Engineering, Faculty of Engineering, Shahid Bahonar University of Kerman, Kerman, Iran
**Young Researchers Society, Shahid Bahonar University of Kerman, Kerman, Iran
(*Received 30 October 2016 • accepted 20 June 2017*)

Abstract−Critical properties and acentric factor (ω) of 31 ionic liquids (ILs) were obtained by using vapor-liquid equilibrium data of solvent+IL consisting of P-T and P-x experimental data, based on three-parameter Patel-Teja equation of state and genetic algorithm. Optimized P_c, T_c and ω of ILs with Peng-Robinson equation of state (PR EoS) were used to model the behavior of phase equilibria of solvent+IL. Due to lack of experimental data for optimized properties, the validation was done by comparing them to the results in the literature. In each comparison the average absolute percent deviation (AAPD) for optimized properties was based on P-T experimental data, with PR EoS was minimum. For more confidence in the correctness of optimized properties, the behavior of phase equilibria of two new mixtures (i.e., water+emimDMP and methanol+emimDMP), the density and vapor pressure of some pure ILs were predicted by PR EoS, which the prediction of this EoS was satisfactory.

Keywords: Patel-Teja, Ionic Liquids, Critical Properties, Acentric Factor, Genetic Algorithm

INTRODUCTION

Ionic liquids (ILs) are a new type of chemical compounds with extraordinary properties that have evolutionary effects on chemical industries and research centers [1-3]. These compounds, which are green chemicals, have an important role in reducing toxic and environmentally harmful substances usage. Ionic liquids' molecular structure is formed by cations and anions [4,5]. Cations are usually large and asymmetric organic compounds, but anions are smaller and more asymmetric and organic or inorganic. Because of this difference in size, the bond between cations and anions is weak and they are liquid at temperatures below 100 °C [6,7]. The most important feature of these compounds is the change in physical properties by changing the cation and anion type. One of the reasons has led to intense research on ILs is to find a proper substitution for volatile organic solvents [4-9]. These solvents are the most important source of biological pollutions in chemical industries. ILs have been highly regarded because of their low vapor pressure. But this does not mean they are all green solvents [1-5]. Some of them are even highly toxic. Non-flammability, being liquid in a wide range of temperature, thermal stability, electrical conductivity, polarity and high density, are some important properties of ILs. Moreover, they are good solvents for both organic and inorganic materials, and polar and non-polar components [10].

All processes should be modeled and designed in pilot scale before the ultimate design or industrial scale run [10-12]. Modelling is used in different sciences to analyze a system. Using a mathematical model to predict the effects of various parameters on a system or a process is much simpler, cheaper and easier than study on a real one [11-14]. Of course, a mathematical model should be used along experimental data. To use ILs on an industrial scale and because of their characteristics, we need some equations to predict their physical, chemical and transport properties [15-17]. Thermodynamics properties have a significant role in engineering designs and developing an accurate model to predict these properties and phase equilibria of pure substance in a wide range of temperature and pressure [16-20]. To model thermodynamics systems, we can use cubic equations of state. These equations require critical pressure (P_c), critical temperature (T_c) and acentric factor (ω) of substance. On the other hand, many researchers have shown that ILs decompose as they approach their boiling point. Critical properties and ω of ILs are not experimentally achievable. Hence, they are considered hypothetically [19-22].

In 2005, Rebelo et al. [23] estimated several ILs critical temperatures by an empirical relation and surface tension and density data. Valderrama et al. in 2007 and 2008 [11,12] calculated the critical properties, boiling point and acentric factor of some ILs by group contribution method based on modified Lydersen-Joback-Reid method concepts, which did not require molecular weight and structure of ILs and checked their results by ILs density. In 2013, Shariati et al. [13] obtained P_c, T_c and ω of 10 ILs using VLE data of binary mixtures of CO_2+IL, PR EoS and differential evolution (DE) optimization algorithm, then by Soave-Redlich-Kwong equation of state (SRK EoS) and optimized properties predicted the bubble point of binary mixtures of CO_2+IL.

Due to the interesting properties of ionic liquids for use in industry, thermodynamics properties of these liquids including crit-

†To whom correspondence should be addressed.
E-mail: amohebbi2002@yahoo.com, amohebbi@uk.ac.ir

ical properties are required. Most ILs decompose before reaching their critical region. Consequently, measurement of their critical properties is not possible experimentally. In this study, P-T data at constant composition (x) and P-x data at constant temperature were used to obtain the critical properties and ω of 31 ILs by Patel-Teja (PT) EoS based on genetic algorithm. Moreover, the optimized critical properties and ω were applied to predict the pure density and vapor pressure of some ILs.

METHODOLOGY

A wide range of thermodynamics models are used to describe the behavior of systems containing ILs [10]. Because of their simplicity and ordinary calculations, cubic EoS have drawn attention. The simplest, and widely successful EoS, is the semi-empirical van der Waals type EoS with two-parameters. After van der Waals, many equations of state have been proposed for the representation of the volumetric properties of pure liquids [24]. These equations, which improved the attractive and repulsive intermolecular forces, were modified by numerous investigators. Other equations with many parameters have also been used to describe the fluid phase behavior, some with reasonable success [14]. The most successful cubic equations for phase equilibrium calculations have been those proposed by Soave. He modified the temperature dependency of the attractive term in Redlich-Kwong EoS (RK EoS) by a more general function α (see Eq. (A4)) and added acentric factor parameter (ω) and proposed the Soave-Redlich-Kwong EoS (SRK EoS). After that, Peng and Robinson modified the attractive term mainly to improve the prediction of liquid density in comparison with SRK EoS and presented the PR EoS. A two-parameter EoS, like SRK and PR EoSs, predicts the fixed critical compressibility factor (i.e. $Z_c=P_cV_c/RT_c$) for all fluids (i.e., 0.307 and 0.333 by PR and SRK, respectively) [14,24]. In fact, actual Z_c values for most fluids are generally smaller than those predicted by either two-parameter EoS. It demonstrates the inflexibility of two-parameter EoS for matching both the vapor pressure and volume leads to unreliable volumetric data at all conditions (i.e., inaccuracy of predicted density of liquid, saturated liquid and at the critical point).

Table 1. The IUPAC name of ILs studied in this work

Abbreviation	Ionic liquid
[bmim][BF_4]	1-Butyl-3-methylimidazolium tetrafluoroborate
[bmim][Cl]	1-Butyl-3-methylimidazolium chloride
[bmim][SCN]	1-Butyl-3-methylimidazolium thiocyanate
[bmim][$OcSO_4$]	1-Butyl-3-methylimidazolium octylsulfate
[emim][FAP]	1-Ethyl-3 methylimidazoliumtris(pentafluoroethyl) trifluorophosphate
[emim][PF_6]	1-Ethyl-3-methylimidazolium hexafluorophosphate
[emim][SCN]	1-Ethyl-3-methylimidazolium thiocyanate
[emim][DMP]	1-Ethyl-3-methylimidazolium dimethylphosphate
[hmim][BF_4]	1-Hexyl-3-methylimidazolium tetrafluoroborate
[hmim][PF_6]	1-Hexyl-3-methylimidazolium hexafluorophosphate
[hmim][$MeSO_4$]	1-Hexyl-3-methylimidazolium methylsulfate
[hmim][TFO]	1-Hexyl-3-methylimidazolium trifluoromethanesulfonate
[emim][Tf_2N]	1-Ethyl-3-methylimidazolium bis(trifluoromethylsulfonyl)imide
[bmim][Tf_2N]	1-Butyl-3-methylimidazolium bis(trifluoromethylsulfonyl)imide
[bmim][DCA]	1-Butyl-3-methylimidazolium dicyanamide
[C_5mim][Tf_2N]	1-Methyl-3-pentylimidazolium bis(trifluoromethylsulfonyl)imide
[C_6mim][Tf_2N]	1-Hexyl-3-methylimidazolium bis[(trifluoromethyl)sulfonyl]imide
[C_8mim][Tf_2N]	1-Octyl-3-methylimidazolium bis[(trifluoromethyl)sulfonyl]imide
[C_3mpy][Tf_2N]	n-Propyl-n-methylpyrrolidiniumbis(trifluoromethylsulfonyl)imide
[C_5mpy][Tf_2N]	n-Pentyl-n-methylpyrrolidiniumbis(trifluoromethylsulfonyl)imide
[C_7mpy][Tf_2N]	n-Heptyl-n-methylpyrrolidiniumbis(trifluoromethylsulfonyl)imide
[C_9mpy][Tf_2N]	n-Nonyl-n-methylpyrrolidiniumbis(trifluoromethylsulfonyl)imde
[dmim][MP]	1,3-Dimethylimidazolium methylphosphonate
[bmp][TFO]	1-Butyl-1-methylpyrrolidinium trifluoromethanesulfonate
[hmp][Tf_2N]	1-Hexyl-1-methylpyrrolidinium bis(trifluoromethylsulfonyl)imide
[omim][BF_4]	1-n-Octyl-3-methylimidazolium tetrafluoroborate
[omp][Tf_2N]	1-Octyl-methylpyrrolidinium bis(trifluoromethylsulfonyl)imide
[tbma][$MeSO_4$]	Tributylmethylammoniummethylsulfate
[tbmp][$MeSO_4$]	Tributylmethylphosphoniummethylsulfate
[$(eto)_2$im][Tf_2N]	1,3-Diethoxyimidazolium bis(trifluoromethylsulfonyl)imide
[$P_{14,6,6,6}$][Tf_2N]	Trihexyltetradecylphosphoniumbis(trifluoro-methylsulfonyl)imide

Therefore, to obtain an acceptable prediction of liquid density, EoS must determine Z_c based on any component. The third parameter reduced the mentioned limitations of two-parameter EoS. This parameter is generally determined by employing volumetric data [24]; therefore, a three-parameter such as Patel-Teja EoS has superior accuracy compared with a two-parameter EoS such as PR EoS. Continuing these efforts, in 1982 Patel and Teja presented the three-parameter cubic EoS. They modified the attractive term by adding parameter c. This parameter in PT EoS, is a kind of specific volume and its concept is similar to the volume transition, which was presented by Peneloux et al. [24].

In this study, $\varphi-\varphi$ approach was used and the fugacity coefficients of each component in vapor and liquid phases were calculated by PT EoS [24]:

$$P=\frac{RT}{v-b}-\frac{a}{v(v+b)+c(v-b)} \quad (1)$$

where a and b are the attractive and repulsive (co-volume) parameters of equation of state respectively. c is flexible third parameter, which is determined from the critical properties and acentric factors for pure components. Various mixing rules can be applied to calculate EoS parameters for a mixture. In the present work, the simple van der Waals (VDW) mixing model was employed to determine the mixture EoS parameters [24]:

Table 2. Critical pressure, critical temperature and acentric factor of ionic liquids and solvents used in this study

No.	IL	T_c (K)	P_c (MPa)	ω	Reference
1	[hmim][$MeSO_4$]	1111.6	2.97	0.4901	a
2	[hmim][TfO]	1056.1	2.50	0.4856	a
3	[emim][DMP]	836.8	2.50	0.6383	a
4	[emim][FAP]	760.4	1.01	0.8743	a
5	[emim][Tf_2N]	1215.3	3.37	0.2878	a
6	[C_5mim [Tf_2N]	1251.2	2.73	0.4194	a
7	[C_6mim][Tf_2N]	877.5	2.22	1.3102	a
8	[C_8mim][Tf_2N]	924.1	1.89	1.3412	a
9	[C_3mpy][Tf_2N]	1197.5	2.66	0.2786	a
10	[C_5mpy][Tf_2N]	1222.5	2.33	0.3638	a
11	[C_7mpy][Tf_2N]	1247.8	2.05	0.4624	a
12	[C_9mpy][Tf_2N]	1278.6	1.83	0.5412	a
13	[tbma][$MeSO_4$]	1001.3	1.96	0.6424	a
14	[tbmp][$MeSO_4$]	1034.7	1.98	0.7201	a
15	[hmp][Tf_2N]	1236.4	2.18	0.4112	a
16	[omp][Tf_2N]	1264.2	1.94	0.5089	a
17	[dmim][MP]	766.8	3.29	0.4758	a
18	[$P_{14,6,6,6}$][Tf_2N]	1605.1	0.86	0.7681	a
19	[bmp][TFO]	934.8	2.60	0.6124	a
20	[$(eto)_2$im][Tf_2N]	1311.2	2.84	0.2852	a
21	[bmim][Tf_2N]	1256	2.76	0.2656	11
22	[bmim][DCA]	1035.8	2.44	0.8419	12
23	[bmim][$OcSO_4$]	1189.8	2.02	0.7042	12
24	[bmim][SCN]	1047.4	1.94	0.4781	12
25	[bmim][Cl]	789.0	2.78	0.4908	12
26	[emim][PF_6]	663.5	1.95	0.6708	11
27	[emim][SCN]	1013.6	2.23	0.3931	12
28	[hmim][BF_4]	679.1	1.79	0.9258	11
29	[hmim][PF_6]	754.3	1.55	0.8352	11
30	[omim][BF_4]	726.1	1.60	0.9954	11
31	[bmim][BF_4]	632.3	2.04	0.8489	11
32	Carbon dioxide	304.2	7.39	0.2240	25
33	Water	647.1	22.05	0.3450	25
34	Ethanol	513.9	6.15	0.6450	25
35	Methanol	512.6	8.09	0.5640	25
36	Styrene	636.0	3.84	0.2970	25
37	Nitrous oxide	309.6	7.25	0.1409	25

a: Calculated from modified Lydersen-Joback-Reid method [See Appendix B.]

$$a = \Sigma_i \Sigma_j z_i z_j \sqrt{a_i a_j}(1 - k_{ij}) \quad (2)$$

$$b = \Sigma_i z_i \frac{b_i + b_j}{2}(1 - l_{ij}) \quad (3)$$

$$c = \Sigma_i z_i c_i \quad (4)$$

where z_i is the mole fraction of component i (in the vapor phase $z_i=y_i$ and in the liquid phase $z_i=x_i$), k_{ij} and l_{ij} are the binary interaction and the repulsive binary interaction parameters respectively. The details of PT and PR EoSs are given in Appendix A. The IUPAC name, P_c, T_c and ω of ILs studied in this work, are given in Tables 1 and 2, respectively. The details of calculations of the critical pressure, the critical temperature and the acentric factor of pure ILs based on the modified Lydersen-Joback-Reid method [11] are given in Appendix B. To calculate ILs critical properties and acentric factor, we need information of their structure. Therefore, we used the ILs structure presented by Valderrama et al. [11,12].

Phase equilibria calculations were based on P-T experimental data at constant x and P-x experimental data at constant temperature. P_c, T_c and ω for 31 ILs were optimized by using the genetic algorithm in MATLAB programming. An objective function was used to optimize these properties and minimize the error. This function is defined as:

$$OF = \Sigma \left| \frac{P_{Exp.} - P_{Calc.}}{P_{Exp.}} \right| \quad (5)$$

where $P_{Exp.}$ and $P_{Calc.}$ are experimental and calculated bubble point

Table 3. Temperature, pressure and solvent solubility ranges of used ionic liquids in this study

No.	System	ndp[a]	Temperature range (K)	Pressure range (MPa)	Solubility range of solvent in IL	Reference
1	emimSCN-Styrene	36	329.70-401.60	0.00297-0.01999	0.087-0.322	27
2	hmimTfO-Carbon dioxide	64	303.15-373.15	1.42-100.12	0.267-0.816	28
3	hmim$MeSO_4$-Carbon dioxide	48	303.15-373.15	0.87-50.14	0.158-0.602	28
4	bmimSCN-Carbon dioxide	56	292.35-384.15	1.05-31.50	0.126-0.43	29
5	dmimMP-Carbon dioxide	26	313.15-363.15	3.4-25.00	0.162-0.475	29
6	$(eto)_2$imTf_2N-Carbon dioxide	36	302.85-363.15	2.115-32.86	0.396-0.812	29
7	emimTf_2N-Carbon dioxide	80	292.16-363.15	0.62-47.85	0.221-0.75	30
8	C_5mimTf_2N-Carbon dioxide	81	298.37-363.29	0.72-59.805	0.212-0.802	30
9	bmimTf_2N-Carbon dioxide	209	292.65-453.15	0.420-49.99	0. 0847-0.801	6,8,31
10	bmimDCA-Carbon dioxide	40	293.36-363.25	1.018-73.64	0.200-0.601	31
11	hmpTf_2N-Carbon dioxide	64	303.15-373.15	1.06-47.55	0.2778-0.8105	32
12	ompTf_2N-Carbon dioxide	72	303.15-373.15	0.51-35.92	0.2409-0.8176	32
13	C_3mpyTf_2N-Carbon dioxide	56	303.15-373.15	0.52-47.10	0.186-0.787	33
14	C_5mpyTf_2N-Carbon dioxide	64	303.15-373.15	0.27-55.10	0.198-0.785	33
15	C_7mpyTf_2N-Carbon dioxide	64	303.15-373.15	0.26-72.24	0.302-0.853	33
16	C_9mpyTf_2N-Carbon dioxide	56	303.15-373.15	0.26-36.58	0.323-0.820	33
17	bmimCl-Carbon dioxide	45	353.15-373.15	2.454-36.946	0.1306-0.406	34
18	bmim$OcSO_4$-Carbon dioxide	52	303.22-368.41	0.982-9.410	0.152-0.45	35
19	$P_{14,6,6,6}Tf_2$N-Carbon dioxide	98	293.35-375.35	0.53-22.20	0.3603-0.8480	6,36
20	bmpTfO-Carbon dioxide	64	303.15-373.35	1.88-70.20	0.2583-0.7058	36
21	emimFAP-Carbon dioxide	50	283.75-364.13	0.447-10.40	0.1003-0.60	16
22	tbma$MeSO_4$-Carbon dioxide	28	338.35-368.63	1.009-11.528	0.066-0.368	37
23	tbmp$MeSO_4$-Carbon dioxide	29	313.16-363.30	0.659-12.640	0.070-0.378	37
24	C_6mimTf_2N-Carbon dioxide	109	298.15-344.55	0.157-39.00	0.039-0.8333	19,20,38
25	C_8mimTf_2N-Carbon dioxide	96	298.35-344.55	0.680-34.80	0.3019-0.8456	38
26	emimDMP-Ethanol	46	309.05-389.15	0.00747-0.0511	0.500-0.89	39
27	emimDMP-Water	43	320.35-411.15	0.00627-0.04356	0.490-0.9	39
28	emimDMP-Methanol	46	301.95-386.15	0.01134-0.04630	0.500-0.89	39
29	emimPF_6-Carbon dioxide	74	308.14-366.03	1.49-97.10	0.104-0.619	40
30	hmimPF_6-Carbon dioxide	98	291.31-363.58	0.64-94.60	0.098-0.727	15,41
31	hmimBF_4-Carbon dioxide	104	293.18-368.16	0.54-86.60	0.103-0.703	42
32	omimBF_4-Carbon dioxide	100	308.20-363.29	0.571-85.80	0.1005-0.7523	43
33	bmimBF_4-Carbon dioxide	104	278.47-368.22	0.587-67.62	0.1022-0.6017	44
34	bmimBF_4-Nitric oxide	42	298.10-323.20	0.0258-2.0532	0.0010-0.2080	18
	Total number of data	2280				

[a]ndp is the number of experimental data point

pressures using PT EoS, respectively. More details of the calculations of critical properties and acentric factor of ILs based on PT EoS and genetic algorithm (GA) are given in Appendix C. In this Appendix, the block diagram of a computer program for bubble point pressure calculations and the details of one step of the calculations are given for one point of the experimental data of CO_2-[bmim][BF_4] binary mixture.

Genetic algorithm (GA) has a wide operational range. With advances in science and technology; it has been used more in optimization and problem solving. Genetic algorithm may be considered a general search method that follows natural biologic evaluation rules. In the algorithm, initially several answers are generated randomly (initial population). After choosing better answers, the new population is generated using genetic algorithm operators. In this process, the new population is better than the old one. Selecting some answers among all to create new ones is based on their utility and is done by the fitness function. It is obvious that more appropriate answers have more chance to reproduce. This procedure continues until the predetermined conditions such as a number of populations or answers improvements are established [10,26]. The systems investigated in this study, include 31 ionic liquids and six solvents. All systems are given in Table 3.

RESULTS AND DISCUSSION

Tables 4 and 5 show the optimized values of P_c, T_c and ω for 31 ILs. These values were obtained based on P-T data at constant x and P-x data at constant temperature for binary mixtures of solvent+IL using PT EoS and GA. The average absolute percent deviation (AAPD) is calculated by Eq. (6):

$$\mathrm{AAPD}=\frac{1}{N}\Sigma_{i=1}^{N}\left|\frac{P_i^{Exp.}-P_i^{Calc.}}{P_i^{Exp.}}\right|\times 100 \tag{6}$$

N is the number of experimental data points for each binary mix-

Table 4. Critical pressure, critical temperature and acentric factor of ILs calculated in this work by PT EoS based on the genetic algorithm optimization method and P-T experimental data at constant x

No.	IL	T_c (K)	P_c (MPa)	ω	AAPD in bubble point pressure prediction
1	[hmim][TfO]	1143.5	3.24	0.3818	3.48
2	[hmim][$MeSO_4$]	1209.7	3.58	0.4697	3.65
3	[bmim][BF_4]	765.4	3.56	0.7956	1.16
4	[bmim][Cl]	803.1	4.68	0.6560	0.82
5	[bmim][$OcSO_4$]	1172.6	2.30	0.8863	1.22
6	[emim][PF_6]	745.7	4.16	0.6436	3.84
7	[dmim][MP]	816.2	4.65	0.5898	10.34
8	[$(eto)_2$im][Tf_2N]	1361.0	3.08	0.2275	5.21
9	[emim][Tf_2N]	1267.7	2.80	0.2578	8.98
10	[bmim][DCA]	954.5	3.16	0.8018	8.88
11	[C_6mim][Tf_2N]	799.1	2.39	0.8702	4.08
12	[C_8mim][Tf_2N]	1187.8	1.02	0.9078	1.93
13	[C_3mpy][Tf_2N]	1227.9	3.23	0.3222	0.85
14	[C_5mpy][Tf_2N]	1313.1	2.65	0.3027	7.39
15	[C_7mpy][Tf_2N]	1329.8	1.89	0.4645	5.22
16	[C_9mpy][Tf_2N]	1339.7	2.08	0.3278	5.70
17	[hmp][Tf_2N]	1316.2	2.33	0.3354	5.02
18	[hmim][BF_4]	798.4	2.97	0.8624	3.89
19	[hmim][PF_6]	847.2	2.59	0.7836	4.10
20	[omp][Tf_2N]	1320.4	1.41	0.3094	3.91
21	[omim][BF_4]	834.5	1.88	0.9864	5.35
22	[bmp][TfO]	1017.8	3.78	0.4689	0.84
23	[tbmp][$MeSO_4$]	1003.6	3.16	0.7778	1.17
24	[tbma][$MeSO_4$]	1085.0	3.02	0.8144	0.78
25	[$P_{14,6,6,6}$][Tf_2N]	1758.7	0.77	0.8131	2.11
26	[emim][FAP]	848.2	1.80	0.5474	6.66
27	[emim][SCN]	1146.6	4.86	0.4514	8.58
28	[bmim][SCN]	1194.8	2.76	0.4362	6.26
29	[emim][DMP]	1075.7	2.27	0.5947	10.48
30	[bmim][Tf_2N]	962.2	2.62	0.3943	3.45
31	[C_5mim][Tf_2N]	1332.1	2.80	0.4451	3.91
	Average AAPD				4.50

Table 5. Critical pressure, critical temperature and acentric factor of ILs calculated in this work by PT EoS based on the genetic algorithm optimization method and P-x experimental data at constant temperature

IL	T_c (K)	P_c (MPa)	ω	AAPD in bubble point pressure prediction
[bmim][BF_4]	955.4	4.14	0.4287	6.66
[emim][PF_6]	948.2	2.57	0.9004	5.71
[hmim][BF_4]	822.7	3.28	0.5524	6.42
[hmim][PF_6]	804.6	2.89	0.8875	8.39
[omim][BF_4]	623.8	1.11	1.1248	7.52
[$P_{14,6,6,6}$][Tf_2N]	1483.9	0.95	0.7045	6.46
[bmim][Tf_2N]	874.5	2.26	0.5498	9.79
[C_6mim][Tf_2N]	645.8	4.33	0.9454	8.19
Average AAPD				7.40

ture (e.g., the whole database, or data for selected ILs). The $P_i^{Exp.}$ and $P_i^{Calc.}$ are experimental and calculated bubble point pressures using PT EoS, respectively. The AAPD values for P_c, T_c and ω of this work based on P-T data at constant x and P-x data at constant temperature are 4.5% and 7.4%, respectively.

Shariati et al. [13] used binary interaction parameter (i.e. k_{ij}) to predict the critical properties and ω for six common ILs, but to use the optimized critical properties for pure ILs systems, we cannot employ k_{ij}. Although using the k_{ij} parameter could reduce a little the values of error, in this study this parameter was not used (k_{ij}=0) to predict the critical properties and ω. Because PT EoS was capable to predict phase behavior well.

To validate our model, the results of the present study were compared with experimental data and other works in literature. For example, Fig. 1 compares the calculated bubble point pressure of CO_2+[hmim][BF_4] mixtures by PR EoS with the van der Waals mixing rules type one (without the use of any repulsive binary interaction parameter, i.e. l_{ij}=0), using optimized P_c, T_c and ω based on PT EoS and those values predicted by PR EoS based on Shariati et al. [13] and Valderrama et al. [11,12] methods. As one can see from this figure, there is a very good agreement between the results of our model and experimental data [42]. Comparison of the results of our optimized properties with Shariati et al. [13] and Valderrama et al. [11,12], shows our optimized properties have the minimum deviation from the experimental data, especially at higher pressure. Lower values of k_{ij} and nonlinear behavior at whole range of pressure are observed. However, the results based on P-T data at constant x, are better accuracy than those values based on P-x data at constant temperature. In the P-T data-set at constant x, the mole fraction of liquid phase is fixed in all stages of the bubble point calculations. Consequently, according to Eqs. (2)-(4) a, b and c parameters of mixture are constant in all iteration stages of the bubble point pressure calculations. In this case, these parameters are only function of T_c, P_c and ω. But in the P-x data-set at constant T, the liquid mole fraction (x) changes by varying the pressure. Therefore, the mentioned parameters (i.e., a, b and c) for a mixture change in all iteration stages of the bubble point calculations.

Tables 6 and 7 also give the results of P_c, T_c and ω prediction for solvent+IL systems using PR EoS based on four methods. These tables list the average absolute percent deviation (AAPD) and k_{ij}

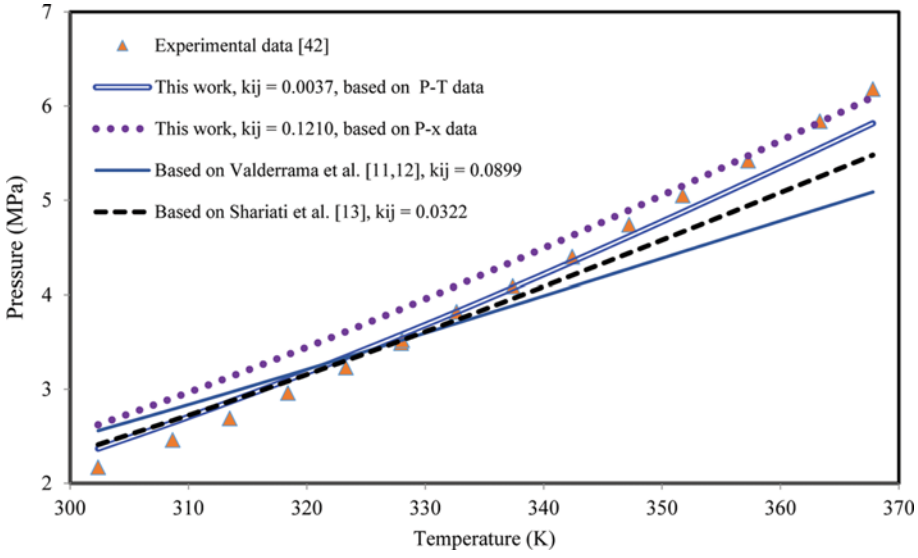

Fig. 1. Comparison of bubble point pressure experimental data with those predicted values by our model and PR EoS based on Valderrama et al. [11,12] and Shariati et al. [13] methods for CO_2+[hmim][BF_4] at x_{CO_2}=0.299.

Table 6. AAPD for bubble point pressure prediction from P-T data at constant x for CO_2+IL systems using PR EoS based on optimized properties, modified Lydersen-Joback-Reid method [11], Shariati et al. method [13] and Valderrama et al. method [11,12]

No.	Ionic liquid	Solubility of solvent in IL	AAPD (Based on optimized properties)	AAPD (Based on modified Lydersen-Joback-Reid method)	AAPD (Based on Shariati et al. method)	AAPD (Based on Valderrama et al. method)	k_{ij} (Based on optimized properties)	k_{ij} (Based on modified Lydersen-Joback-Reid method)	k_{ij} (Based on Shariati et al. method)	k_{ij} (Based on Valderrama et al. method)
1	hmimTFO	0.6390	3.63	8.01	-	-	0.0071	0.0381	-	-
2	hmimMeSO$_4$	0.5730	3.87	7.21	-	-	0.0111	0.0949	-	-
3	dmimMP	0.3690	7.40	15.40	-	-	0.0659	0.1740	-	-
4	(eto)$_2$imTf$_2$N	0.5540	5.72	6.98	-	-	0.0027	0.0075	-	-
5	emimTf$_2$N	0.6060	4.15	7.68	-	-	−0.0112	−0.0263	-	-
6	C$_5$mimTf$_2$N	0.4530	1.73	7.85	-	-	−0.0370	−0.0684	-	-
7	hmpTf$_2$N	0.3827	5.64	8.52	-	-	−0.0011	−0.0123	-	-
8	ompTf$_2$N	0.4424	3.94	6.16	-	-	−0.0155	−0.0455	-	-
9	C$_3$mpyTf$_2$N	0.5610	0.88	4.65	-	-	0.0041	0.04028	-	-
10	C$_5$mpyTf$_2$N	0.3300	7.94	11.87	-	-	0.0014	0.0128	-	-
11	C$_7$mpyTf$_2$N	0.5910	5.68	7.23	-	-	−0.0035	−0.0063	-	-
12	C$_9$mpyTf$_2$N	0.7210	6.02	10.02	-	-	−0.0061	−0.0119	-	-
13	P$_{14,6,6,6}$Tf$_2$N	0.7099	2.11	4.02	-	-	−0.0155	−0.0189	-	-
14	bmpTfO	0.2583	1.08	5.46	-	-	0.0089	0.0581	-	-
15	emimFAP	0.3012	4.84	11.03	-	-	−0.0201	0.0631	-	-
16	tbmaMeSO$_4$	0.3680	0.58	5.69	-	-	0.0106	0.1266	-	-
17	tbmpMeSO$_4$	0.4550	0.75	4.96	-	-	0.0091	0.0894	-	-
18	C$_6$mimTf$_2$N	0.6681	2.23	7.50	-	-	−0.0546	−0.1051	-	-
19	C$_8$mimTf$_2$N	0.4849	1.89	9.25	-	-	−0.0614	−0.1018	-	-
20	bmimTf$_2$N	0.3818	2.09	-	5.43	5.33	0.0220	-	0.0126	−0.0204
21	emimPF$_6$	0.3560	4.01	-	6.14	11.29	0.0100	-	0.0976	0.1199
22	hmimPF$_6$	0.5010	4.46	-	7.89	9.91	0.0062	-	0.06867	0.1001
23	hmimBF$_4$	0.2990	4.03	-	5.83	9.08	0.0037	-	0.0322	0.0899
24	omimBF$_4$	0.5050	5.62	-	7.15	9.11	0.0032	-	0.0348	0.0882
25	bmimBF$_4$	0.1998	3.15	-	6.48	12.52	0.0050	-	0.0851	0.1041
26	bmimCl	0.2652	0.90	-	-	9.16	0.0123	-	-	0.1769
27	bmimOcSO$_4$	0.4500	0.93	-	-	2.23	0.0051	-	-	0.0223
28	bmimSCN	0.2540	1.08	-	-	5.56	0.0954	-	-	0.1588
29	bmimDCA	0.6010	9.46	-	-	16.99	0.0122	-	-	0.0985
30	emimDMP-Ethanol	0.5000	1.19	8.91	-	-	−0.1214	−0.1691	-	-
31	emimSCN-Styrene	0.1760	9.74	-	-	13.28	0.0018	-	-	0.0825
	Average AAPD		3.77	7.92	6.49	9.50				

for these methods. According to Table 6, the least values of AAPD and k_{ij} for all binary mixtures of solvent+IL were obtained for our work. The close agreement between our results and the experimental data is more obvious in error percent as given in the table. Table 7 shows the results of modelling of CO_2+IL by PR EoS based on optimized properties using P-x data at constant temperature. The AAPD and k_{ij} values for this method are more than the optimization method using P-T data at constant x.

For a fair comparison and investigation of the accuracy of the critical properties obtained from the modelling based on the bubble point experimental data, two systems were considered: mixtures and pure substances. Of course, these systems are new and we did not use them in our optimization stage. At first, P-T behavior of binary solvent+IL system at constant x and P-x behavior of the binary solvent+IL system at constant temperature were investigated. For this purpose, based on P-T data, phase behaviors of water+[emim][DMP] and methanol+[emim][DMP] mixtures were modeled by PR EoS by using the van der Waals mixing rules type two (with the use of repulsive binary interaction parameter, i.e., $l_{ij}\neq 0$), and applying optimized P_c, T_c and ω based on PT EoS (our model), and those values predicted by PR EoS based on modified Lydersen-Joback-Reid method [11]. The results are shown in Fig. 2 and Table 8. As one can see from this figure, there is a very good agreement between our model and experimental data [39]. To ob-

Table 7. AAPD for bubble point pressure prediction from P-x data at constant temperature for CO_2+IL systems using PR EoS based on optimized properties

Ionic liquid	Temperature (K)	AAPD	k_{ij}
$emimPF_6$	332.83	5.92	0.1024
$hmimPF_6$	333	8.66	0.1102
$hmimBF_4$	340	7.37	0.1210
$omimBF_4$	360	8.26	0.1141
$bmimBF_4$	320	6.15	0.1262
$bmimTf_2N$	323	8.48	0.0980
C_6mimTf_2N	343.15	12.28	0.1148
$P_{14,6,6,6}Tf_2N$	353.15	14.57	0.1098
Average AAPD		8.97	

tain a better evaluation of the results of the optimization, the optimized P_c, T_c and ω of [emim][DMP], which were obtained for binary ethanol+[emim][DMP] system using the experimental data, were used to predict the phase behavior of water+[emim][DMP] and methanol+[emim][DMP] systems. In this case, because water and methanol are polar solvents, the behavior of binary systems is non-ideal. Consequently, to decrease the error and improve the accuracy of the chosen model (i.e., PR EoS), the l_{ij} parameter is used, in addition to k_{ij}.

Fig. 3 shows the results of modelling of nitric oxide (N_2O)+[bmim][BF_4] binary system at 298.1 K, using PR EoS based on optimized critical properties and ω for four methods: our two methods (i.e., optimized critical properties based on P-T data at constant x and P-x data at constant temperature), Valderrama et al.

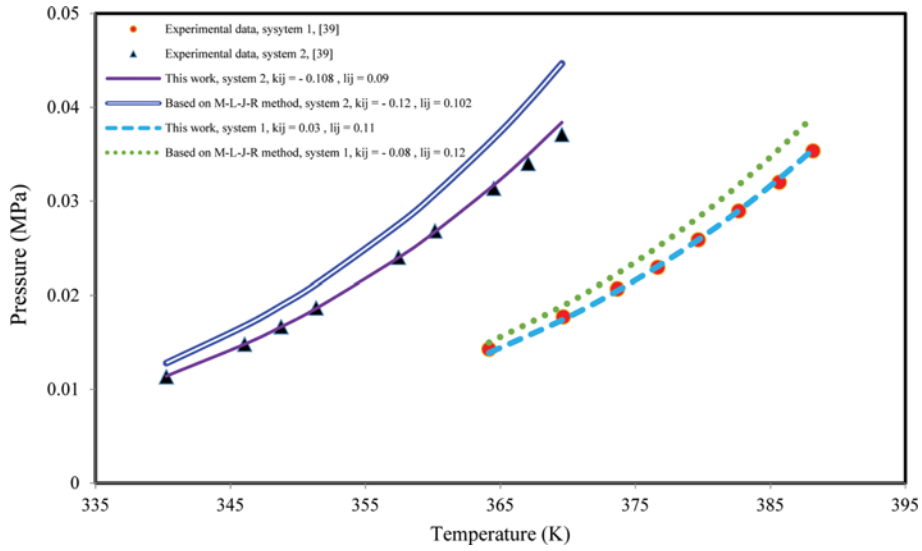

Fig. 2. Comparison of bubble point pressure experimental data using PR EoS, by our model and modified Lydersen-Joback-Reid method for: system 1 (water+[emim][DMP] at $x_{emimDMP}$=0.3) and system 2 (methanol+[emim][DMP] at $x_{emimDMP}$=0.41).

Table 8. AAPD for bubble point pressure prediction from P-T experimental data at constant x for solvent+[emim][DMP] system [39], using PR EoS based on optimized properties and modified Lydersen-Joback-Reid method [11]

Solvent	$x_{emimDMP}$	AAPD (Based on optimized properties)	AAPD (Based on modified Lydersen-Joback-Reid method)	k_{ij} (Based on optimized properties)	l_{ij} (Based on optimized properties)	k_{ij} (Based on modified Lydersen-Joback-Reid method)	l_{ij} (Based on modified Lydersen-Joback-Reid method)
Water	0.51	3.12	12.80	0.08	0.12	0.07	0.13
	0.4	6.02	15.04	0.04	0.09	0.09	0.08
	0.3	5.18	14.65	0.03	0.11	−0.08	0.12
	0.2	7.98	17.48	0.06	0.07	−0.05	0.14
	0.1	8.45	18.79	0.10	0.12	−0.09	0.11
	Average AAPD	6.15	15.76				
Methanol	0.5	4.24	10.35	−0.10	0.101	−0.13	0.08
	0.41	5.86	12.86	−0.108	0.09	−0.12	0.102
	0.3	9.25	18.08	0.12	0.07	−0.09	0.04
	0.2	8.11	22.91	−0.09	0.05	−0.15	0.11
	0.11	12.52	25.27	−0.12	0.11	−0.14	0.12
	Average AAPD	8.00	17.90				

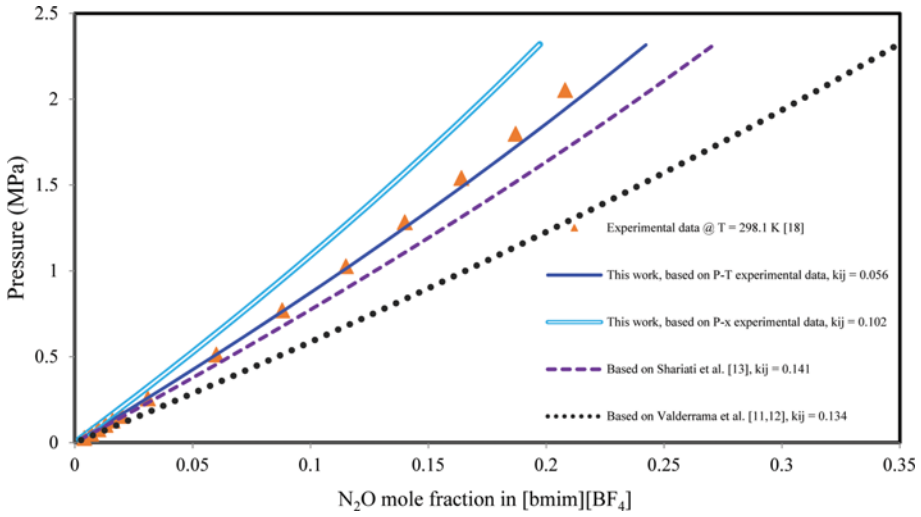

Fig. 3. Isothermal P-x (pressure-solvent composition) phase diagram of N_2O-[bmim][BF_4] binary system, predicted by the PR EoS, based on our model, Valderrama et al. [11,12] and Shariati et al. [13] methods.

Table 9. AAPD for bubble point pressure (P-x experimental data at constant temperature) prediction for N_2O+[bmim][BF_4] system [18], using PR EoS based on optimized properties, Shariati et al. method [13] and Valderrama et al. method [11,12]

Temperature (K)	AAPD (Optimized properties based on P-T experimental data)	AAPD (Optimized properties based on P-x experimental data)	AAPD (Based on Shariati et al. method)	AAPD (Based on Valderrama et al. method)	k_{ij} (Optimized properties based on P-T experimental data)	k_{ij} (Optimized properties based on P-x experimental data)	k_{ij} (Based on Shariati et al. method)	k_{ij} (Based on Valderrama et al. method)
298.1	5.26	11.86	16.75	24.87	0.056	0.102	0.141	0.134
348.1	6.03	10.65	18.05	19.48	0.072	0.098	0.130	0.138
323.2	6.98	9.24	22.41	27.02	0.101	0.120	0.132	0.164
Average AAPD	6.09	10.59	19.07	23.79				

Table 10. AAPD for liquid densities calculated for pure ILs at various pressures and temperatures, using PR EoS based on optimized properties (this work), Shariati et al. method [13] and Valderrama et al. method [11,12]

IL	ndp[a]	AAPD (Optimized properties based on P-T experimental data)	AAPD (Optimized properties based on P-x experimental data)	AAPD (Based on Shariati et al. method)	AAPD (Based on Valderrama et al. method)	Pressure range (MPa)	Temperature range (K)	Reference
[bmim][BF_4]	45	0.46	0.75	2.16	3.75	0.21-39.85	298.15-373.15	45
[hmim][PF_6]	77	1.52	2.14	4.58	6.98	0.1-10	293.15-393.15	46
[emim][PF_6]	180	7.68	10.59	16.77	20.51	10-200	312.8-472.40	47
[hmim][BF_4]	117	1.82	3.24	5.64	9.64	0.1-60	283.15-323.15	48
[bmim][Tf_2N]	80	0.65	1.58	3.81	5.58	0.1	292.88-391.28	49,51
[omim][BF_4]	17	1.17	3.04	7.22	9.55	0.1	283.15-363.15	50
[bmim][$OcSO_4$]	169	8.96	-	-	19.14	10-200	312.19-472.60	52
[emim][SCN]	75	0.68	-	-	4.42	0.1-10	298.15-338.15	21
[bmim][SCN]	75	0.78	-	-	2.12	0.1-10	298.15-338.15	21
[bmim][DCA]	71	3.25	-	-	7.92	0.1	293.15-363.15	51
[bmim][Cl]	6	0.89	-	-	2.35	0.1	348.15-373.15	53
Total number of data	912							
Average AAPD		2.54	3.56	6.70	8.36			

[a]ndp is the number of experimental data point

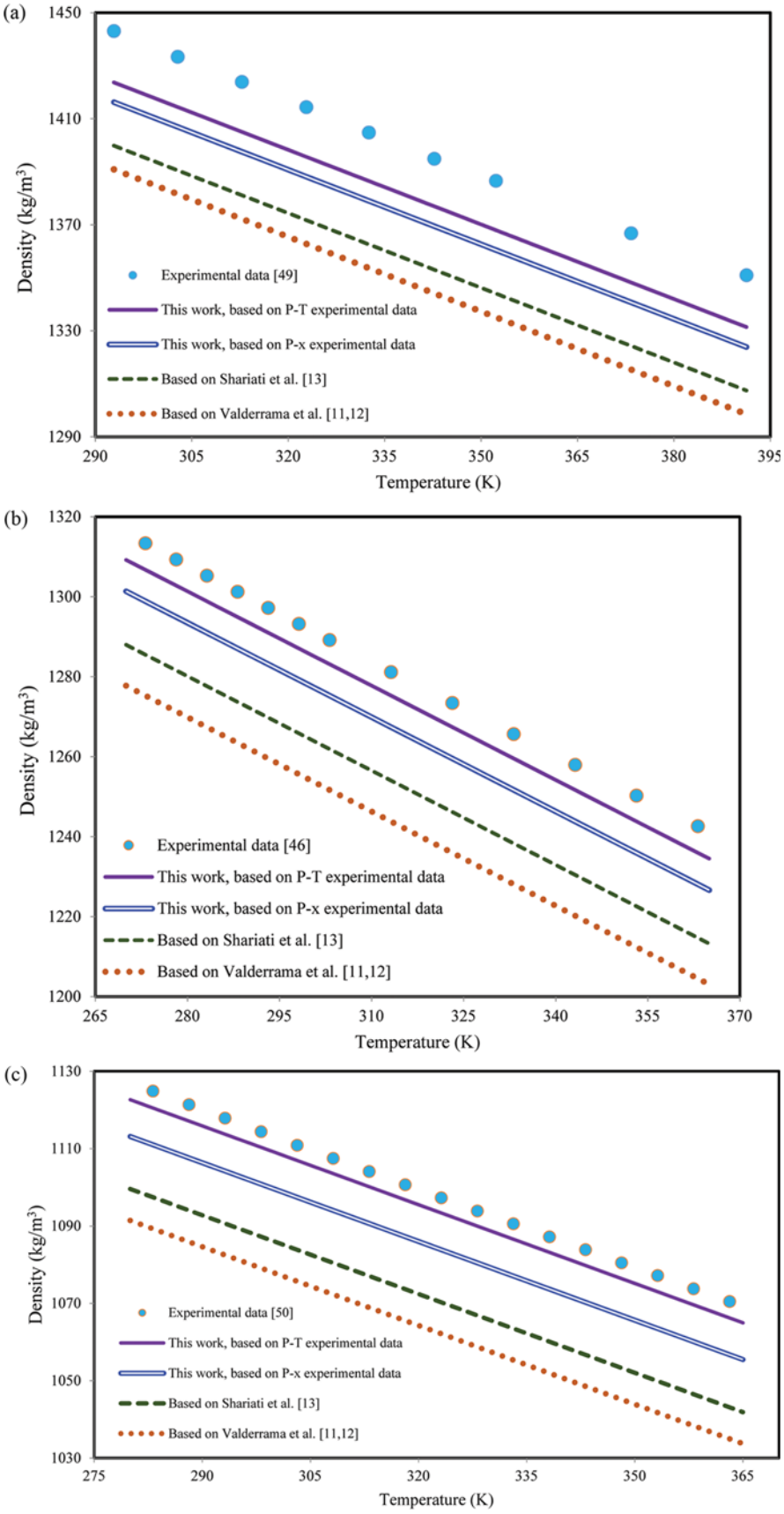

Fig. 4. Prediction of pure ILs density at atmospheric pressure and temperature ranges of 273.15-391.28 K, using PR EoS: (a) [bmim][Tf_2N]. (b) [hmim][PF_6]. (c) [omim][BF_4].

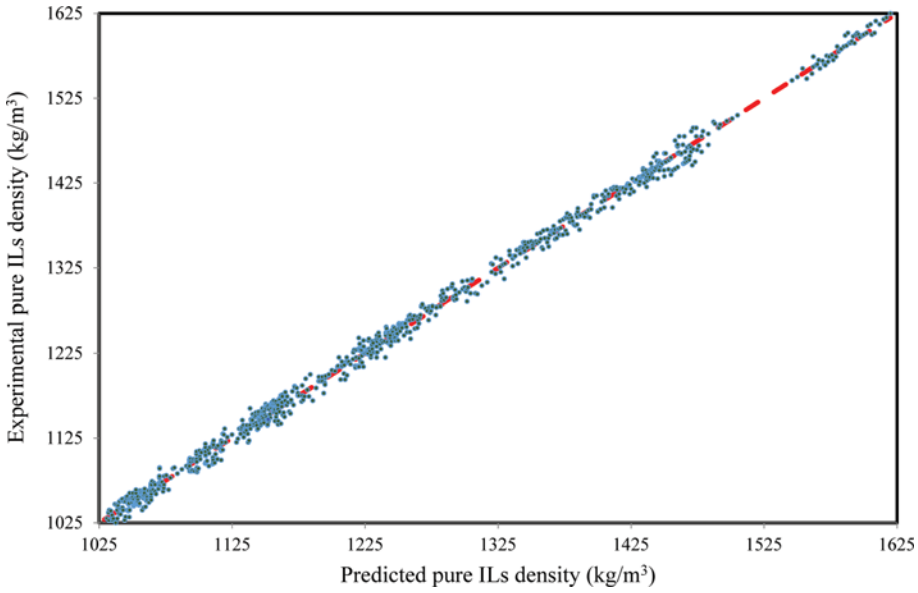

Fig. 5. Plot of experimental density vs. predicted density for pure ILs.

[11,12] and Shariati et al. [13] methods. As one can see, the PR EoS at low pressure and low mole fraction of N_2O was able to predict the behavior of the system based on four methods of estimation of critical properties and ω very well. With increasing the pressure, the deviation from the experimental data [18] increases. But our two methods, especially the optimized method based on P-T data at constant x, have superior accuracy at high pressure. The modelling results of other temperatures and their AAPD are listed in Table 9. As one can see, our two models give the least values of AAPD.

Optimized properties can be used to predict the phase behavior of pure ILs in addition to their application for estimating the phase behavior of mixtures. Therefore, the optimized critical properties and ω were used to calculate the density and vapor pressure of several pure ILs.

Density is a design parameter and effective in mass flow rate calculation. There are several empirical equations based on the critical properties and ω to predict the ILs density. The accuracy of these equations is less than the cubic equation of state. Subsequently, in this study, PR EoS was used to predict the ILs density. This EoS requires the critical properties, ω and the molecular weight for density prediction of pure ILs. For this prediction, the optimized critical properties and ω from this work, the reported critical properties and ω from Valderrama et al. and Shariati et al. were used. The results are given in Table 10.

Moreover, to investigate the accuracy of our optimization method, the variations of density versus temperature at atmospheric pressure for different pure ILs (i.e. [bmim][Tf_2N], [hmim][PF_6], [omim][BF_4]) were predicted and are shown in Fig. 4. The results show that the PR EoS using optimized thermodynamic properties improved the ρ-T behavior of pure ILs. As one can see from Table 10 and the figure, the errors for both our model results were less than other methods and our models succeeded to give better results. Of course, the error for [emim][PF_6] and [bmim][$OcSO_4$] systems was more than other systems due to their high pressure. In high pressures, inter molecular forces are very important and cubic EoS in these ranges of pressure cannot predict the phase behavior well enough. To clarify the procedure of calculations, an example of the step-by-step calculations for [bmim][DCA] density based on PR EoS is given in Appendix C. Moreover, Fig. 5 shows the plot of calculated pure IL density based on the PR EoS using optimized properties versus experimental data (917 data points) and distribution of relative deviations between the calculated values and experimental data. The dashed line is a diagonal line. According to this figure, the PR EoS has good accuracy and could predict ILs density as well.

Vapor pressure was the second property of ILs, which was calculated by PR EoS based on optimized critical properties. The results are shown in Fig. 6 and Table 11. In this case, the vapor pressures of four ILs were estimated and compared with experimental data [54]. The results show PR EoS using optimized properties based on P-T experimental data has a minimum value of AAPD with respect to other methods. An example of the step-by-step calculations for pure [C_8mim][Tf_2N] vapor pressure based on PR EoS is given in Appendix C.

According to Figs. 4 and 6 the PR EoS using optimized T_c, P_c and ω based on P-T experimental data (as best optimization method) could not predict the pure ILs density and vapor pressure appropriately. The main reason of under- and overestimating of these properties is their two-parameter nature [55-57]. Intermolecular forces are very important in ILs liquids, and the main problem of two-parameter cubic EoS like PR EoS is liquid density prediction. This weakness is attributed to the way in which the two EoS parameters, a and b, are calculated. For a pure compound, these parameters are calculated by using critical temperature and pressure [57]. As previously mentioned, a two-parameter EoS yields a constant critical compressibility factor, Z_c, for all fluids, and this typically results in significant errors in liquid-phase densities and vapor pressures. As a result, the ability of two-parameter EoS to predict liquid density is not satisfactory. The study tried to correct

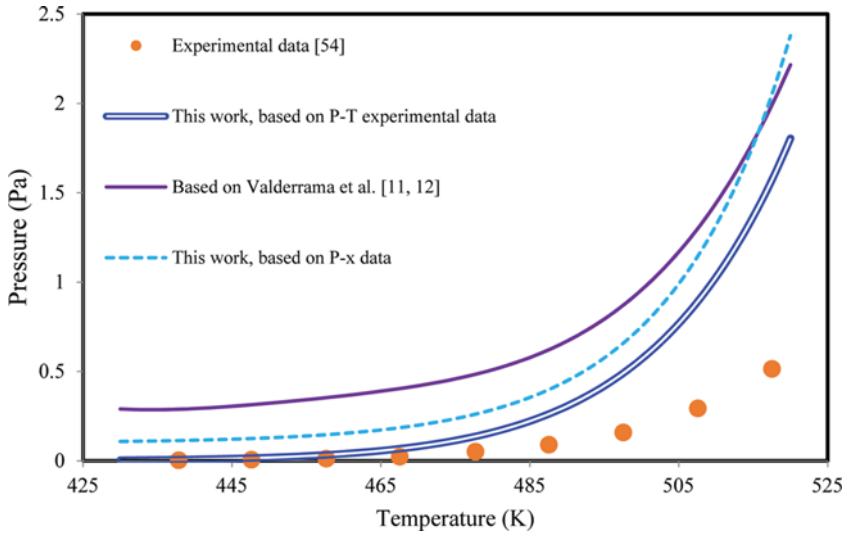

Fig. 6. Prediction of [bmim][Tf_2N] vapor pressure using PR EoS.

Table 11. AAPD for vapor pressure calculated for pure ILs (experimental data [54]) using PR EoS based on optimized properties (this work), Valderrama et al. method [11,12] and modified Lydersen-Joback-Reid method [11]

IL	ndp[a]	AAPD (Optimized properties based on P-T experimental data)	AAPD (Optimized properties based on P-x experimental data)	AAPD (Based on Valderrama et al. method)	AAPD (Based on modified Lydersen-Joback-Reid method)	Pressure range (Pa)	Temperature range (K)
[bmim][Tf_2N]	9	6.48	9.23	16.18	-	0.0036-0.515	437.84-517.45
[emim][Tf_2N]	9	6.08	-	-	14.45	0.0062-0.1091	441.70-484.16
[C_6mim][Tf_2N]	9	5.61	8.12	-	15.70	0.0067-0.1716	445.79-493.67
[C_8mim][Tf_2N]	7	7.43	-	-	19.87	0.0078-0.1542	455.46-498.19
Total number of data	34						
Average AAPD		6.40	8.68	16.18	16.68		

[a]ndp is the number of experimental data point

the critical properties and ω, but because of the two-parameter nature, there is a systematic deviation in density and vapor pressure ILs prediction.

CONCLUSIONS

Because of the unexpected properties of ILs, determination of the critical properties and ω of these liquids is not possible experimentally. The group contribution method and using the phase behavior experimental data of solvent+ILs mixtures are two methods that are proposed.

In this study, PT EoS was combined with genetic algorithm to predict critical temperature, critical pressure and acentric factor of 31 ILs using experimental bubble point pressure of solvent+IL mixtures. P-T experimental data at constant x as well as P-x experimental data at constant temperature for solvent+ILs mixtures were used to obtain these properties. Moreover, by using group contribution method based on concepts of Lydersen-Joback-Reid, these critical properties and ω were obtained. Because of the lack of experimental data for critical properties and ω of ILs, our results were compared with the results of Valderrama et al. and Shariati et al. based on two-parameter PR EoS. The results showed that the optimized properties in this study, especially optimized properties based on P-T experimental data at constant x, have more coincidence with experimental vapor-liquid equilibrium data of binary mixtures of solvent+ILsystem. Obviously, optimized properties based on P-x experimental data at constant temperature also give better results than the calculated properties by Valderrama et al. and Shariati et al. This coincidence especially is more observable in binary systems of water+[emim][DMP], methanol+[emim][DMP] and N_2O+[bmim][BF_4]. Furthermore, to investigate the accuracy of optimized properties with respect to reported properties by Valderrama et al. and Shariati et al., the density and vapor pressure of pure ILs were predicted. The results confirm that our two models predict these ILs properties accurately. According to the results of calculating bubble point pressure for new binary mixture, density and vapor pressure for pure IL and because of the least values of AAPD based on P-T data at constant x, it can be concluded that the method based on the optimized critical properties and acentric factor using P-T data at constant x has good accuracy. Therefore,

this confirms the reliability and validity of the applied method. Therefore, it is possible to find critical properties and ω of pure ILs by heuristic optimization methods based on experimental equilibrium data and use them for modelling different systems.

NOMENCLATURE

a : attractive term parameter of equation of state
A : dimensionless parameter, Eq. (A.15)
AAPD : average absolute percent deviation [-]
b : repulsive term(co-volume) parameter of equation of state [m^3/kgmol]
B : dimensionless parameter Eq. (A16)
c : flexible third parameter [m^3/kgmol]
C : dimensionless parameter Eq. (A17)
Calc. : calculation
Exp. : experimental
i : component i
j : component j
L : liquid
K_i : K-value, Eq. (C7)
k_{ij} : binary interaction parameter [-]
l_{ij} : repulsive binary interaction parameters [-]
M_W : molecular weight [g/mol]
N : number of data point [-]
OF : objective function
P : pressure [MPa]
P^{sat} : vapor pressure [Pa]
P_c : critical pressure [MPa]
R : ideal gas constant [MPa·m^3/K·kgmol]
T : temperature [K]
T_b : normal boiling point [K]
T_c : critical temperature [K]
V : vapor
ν : molar volume [m^3/kgmol]
x : mole fraction in liquid phase [-]
y : mole fraction in vapor phase [-]
z : mole fraction [-]
Z : compressibility factor [-]
Z_c : critical compressibility factor [-]
η : adjusted critical compressibility factor [-]
φ : fugacity coefficient [-]
ω : acentric factor [-]
Σ : sigma

REFERENCES

1. W. Ochędzan-Siodłak, K. Dziubek and D. Siodłak, *J. Mol. Liq.*, **177**, 85 (2013).
2. P. Díaz-Rodríguez, J. C. Cancilla, G. Matute and J. S. Torrecilla, *J. Ind. Eng. Chem.*, **21**, 1350 (2015).
3. F. M. Maia, I. Tsivintzelis, O. Rodriguez, E. A. Macedo, G. M. Kontogeorgis, *Fluid Phase Equilib.*, **332**, 128 (2012).
4. K. N. Marsh, A. Deer, A. C.-T. Wu, E. Tran and A. Klamt, *Korean J. Chem. Eng.*, **19**, 357 (2002).
5. D.-J. Oh and B.-C. Lee, *Korean J. Chem. Eng.*, **23**, 800 (2006).
6. P. F. Requejo, E. J. González, E. A. Macedo and Á. Domínguez, *J. Chem. Thermodynam.*, **74**, 193 (2014).
7. D. L. Minnick and A. M. Scurto, *Fluid Phase Equilib.*, **365**, 11 (2014).
8. S. Raeissi and C. J. Peters, *J. Chem. Eng. Data*, **54**, 382 (2009).
9. J. Dhanalakshmi, P. S. T. Sai and A. R. Balakrishnan, *Ind. Eng. Chem. Res.*, **52**, 16396 (2013).
10. M. R. Sheikhi-Kouhsar, H, Bagheri and S. Raeissi, *Fluid Phase Equilib.*, **395**, 51 (2015).
11. J. O. Valderrama and P. A. Robles, *Ind. Eng. Chem. Res.*, **46**, 1338 (2007).
12. J. O. Valderrama, W. W. Sanga and J. A. Lazzu´s, *Ind. Eng. Chem. Res.*, **47**, 1318 (2008).
13. A. Shariati, S. S. Ashrafmansouri, M. Haji Osbuei and B. Hooshdaran, *Korean J. Chem. Eng.*, **30**, 187 (2013).
14. N. C. Patel and A. S. Teja, *Chem. Eng. Sci.*, **37**, 463 (1982).
15. M. T. Mota-Martinez, M. Althuluth, M. C. Kroon and C. J. Peters, *Fluid Phase Equilib.*, **332**, 35 (2012).
16. M. Althuluth, M. T. Mota-Martinez, M. C. Kroon and C. J. Peters, *J. Chem. Eng. Data*, **57**, 3422 (2012).
17. M. S. Manic, A. J. Queimada, E. A. Macedo and V. Najdanovic-Visak, *J. Supercrit. Fluids*, **65**, 1 (2012).
18. M. B. Shiflett, A. M. S. Niehaus and A. Yokozeki, *J. Phys. Chem. B.*, **115**, 3478 (2011).
19. Y. S. Kim, W. Y. Choi, J. H. Jang, K.-P. Yoo and C. S. Lee, *Fluid Phase Equilib.*, **228-229**, 439 (2005).
20. Y. S. Kim, J. H. Jang, B. D. Lim, J. W. Kang and C. S. Lee, *Fluid Phase Equilib.*, **256**, 70 (2007).
21. M. Kròlikowska and T. Hofman, *Thermochim. Acta*, **530**, 1 (2012).
22. Q. Xin, G. G. Poon and J. M. Prausnitz, *J. Supercrit. Fluids*, **55**, 817 (2010).
23. L. P. Rebelo, J. N. Canongia, J. M. Esperanca and E. Filipe, *J. Phys. Chem. B.*, **109**, 6040 (2005).
24. A. Danesh, PVT and Phase Behaviour of Petroleum Reservoir Fluids, Elsevier B.V. (1998).
25. R. H. Perry and D. W. Green, Perry's Chemical Engineering Handbook, McGraw Hill, New York (2008).
26. R. K. Sahoo, T. Banrjee, S. A. Ahmad and A. Khanna, *Fluid Phase Equilib.*, **239**, 107 (2006).
27. M. T. G. Jongmans, B. Schuur and A. B. de Haan, *J. Chem. Thermodynam.*, **47**, 234 (2012).
28. J.-H. Yim and J. S. Lim, *Fluid Phase Equilib.*, **352**, 67 (2013).
29. A.-H. Revelli, F. Mutelet and J.-N. Jaubert, *J. Phys. Chem. B.*, **114**, 12908 (2010).
30. P. J. Carvalho, V. H. Álvarez, J. J. B. Machado, J. Pauly, J.-L. Daridon, I. M. Marrucho, M. Aznar and J. A. P. Coutinho, *J. Supercrit. Fluids*, **48**, 99 (2009).
31. P. J. Carvalho, V. H. Álvarez, I. M. Marrucho, M. Aznar and J. A. P. Coutinho, *J. Supercrit. Fluids*, **50**, 105 (2009).
32. J.-H. Yim, H. N. Song, B.-C. Lee and J. S. Lim, *Fluid Phase Equilib.*, **308**, 147 (2011).
33. S. A. Kim, J.-H. Yim and J. S. Lim, *Fluid Phase Equilib.*, **332**, 28 (2012).
34. S. Jang, D.-W. Cho, T. Im and H. Kim, *Fluid Phase Equilib.*, **299**, 216 (2010).
35. H. Machida, R. Taguchi, Y. Sato, L. J. Florusse and C. J. Peterrs,

Chem. Eng. China, **3**, 12 (2009).
36. H. N. Song, B.-Ch. Lee and J. S. Lim, *J. Chem. Eng. Data*, **55**, 891 (2010).
37. M. Ramdin, J. H. Vlugt and T. W. de Loos, *J. Chem. Eng. Data*, **57**, 2275 (2012).
38. E.-K. Shin, B.-Ch. Lee and J. S. Lim, *J. Supercrit. Fluids*, **45**, 282 (2008).
39. J. Ren, Z. Zhao and X. Zhang, *J. Chem. Thermodynam.*, **43**, 576 (2011).
40. A. Shariati and C. J. Peters, *J. Supercrit. Fluids*, **29**, 43 (2004).
41. A. Shariati and C. J. Peters, *J. Supercrit. Fluids*, **30**, 139 (2004).
42. M. Costantini, V. A. Toussaint, A. Shariati, C. J. Peters and I. Kikic, *J. Chem. Eng. Data*, **50**, 52 (2005).
43. K. I. Gutkowski, A. Shariati and C. J. Peters, *J. Supercrit. Fluids*, **39**, 187 (2006).
44. M. C. Kroon, A. Shariati, M. Costantini, J. V. Spronsen, G.-J. Witkamp, R. A. Sheldon and C. J. Peters, *J. Chem. Eng. Data*, **50**, 173 (2005).
45. A. Tekin, J. Safarov, A. Shahverdiyev and E. Hassel, *J. Mol. Liq.*, **136**, 177 (2007).
46. R. L. Gardas, M. G. Freire, P. J. Carvalho, I. M. Marrucho, I. M. A. Fonseca, A. G. M. Ferreira and J. A. P. Coutinho, *J. Chem. Eng. Data*, **52**, 80 (2007).
47. R. Taguchi, H. Machida, Y. Sato and R. L. Smith, Jr., *J. Chem. Eng. Data*, **54**, 22 (2009).
48. Y. A. Sanmamed, D. González-Salgado, J. Troncoso, L. Romani, A. Baylaucq and C. Boned, *J. Chem. Thermodynam.*, **42**, 553 (2010).
49. J. Jacquemin, P. Husson, A. A. H. Padua and V. Majer, *Green Chem.*, **8**, 172 (2006).
50. B. Mokhtarani, M. J. Mojtahedi, H. R. Mortaheb, M. Mafi, F. Yazdani and F. Sadeghian, *J. Chem. Eng. Data*, **53**, 677 (2008).
51. C. A. Nieto de Castro, E. Langa, A. L. Morais, M. L. Matos Lopes, M. J. V. Lourenco, F. J. V. Santos, M. S. C. S. Santos, J. N. C. Lopes, H. I. M. Veiga, M. Macatrão, J. M. S. S. Esperancça, C. S. Marques, L. P. N. Rebelo and C. A. M. Afonso, *Fluid Phase Equilib.*, **294**, 157 (2010).
52. H. Machida, Y. Sato and R. L. Smith, Jr., *Fluid Phase Equilib.*, **264**, 147 (2008).
53. H. Machida, R. Taguchi, Y. Sato and R. L. Smith, Jr., *J. Chem. Eng. Data*, **56**,923 (2011).
54. D. H. Zaitsau, G. J. Kabo, A. A. Strechan, Y. U. Paulechka, A. Tschersich, S. P. Verevkin and A. Heintz, *J. Phys. Chem. A.*, **110**, 7303 (2006).
55. J. J. Martin, *Ind. Eng. Chem. Fundam.*, **18**, 81 (1979).
56. A. Peneloux, E. Rauzy and R. Freze, *Fluid Phase Equilib.*, **8**, 7 (1982).
57. M. Nazarzadeh and M. Moshfeghian, *Fluid Phase Equilib.*, **337**, 214 (2013).

APPENDIX A

In this study, the fugacity coefficient of each component in vapor and liquid phases was found by using the pressure-explicit PT EoS [24]:

$$P=\frac{RT}{v-b}-\frac{a_c\cdot\alpha(T)}{v(v+b)+c(v-b)} \tag{A1}$$

where v is the molar volume and R is the universal gas constant. The pure component parameters a_c, b_i and c_i are calculated by the following equations [24]:

$$a_c=\Omega_{aci}\frac{(RT_{ci})^2}{P_{ci}} \tag{A2}$$

$$m_i=0.452413+1.30982\omega_i-0.295937\omega_i^2 \tag{A3}$$

$$\alpha(T)=\left[1+m_i\left(1-\sqrt{\frac{T}{T_{ci}}}\right)\right]^2 \tag{A4}$$

$$b_i=\Omega_{bi}\frac{RT_{ci}}{P_{ci}} \tag{A5}$$

$$c_i=\Omega_{ci}\frac{RT_{ci}}{P_{ci}} \tag{A6}$$

$$\Omega_{ci}=1-3\eta_i \tag{A7}$$

η_i is an adjusted critical compressibility factor, determined by matching the predicted and measured saturated liquid densities. It was correlated with the acentric factor as [24]:

$$\eta_i=0.329032-0.076799\omega_i+0.0211947\omega_i^2 \tag{A8}$$

$$\Omega_{bi}^3+(2-3\eta_i)\Omega_{bi}^2+3\eta_i^2\Omega_{bi}-\eta_i^3=0 \tag{A9}$$

$$\Omega_{aci}=3\eta_i^2+3(1-2\eta_i)\Omega_{bi}+\Omega_{bi}^2+(1-3\eta_i) \tag{A10}$$

where ω_i, T_{ci} and P_{ci} are the acentric factor, critical temperature and critical pressure of component i. Also, the coefficients a, b and c for mixtures are calculated by Eqs. (2)-(4). Moreover, the fugacity coefficient of the solvent in each phase is obtained by [14]:

$$\ln\hat{\phi}_i=-\ln\left(Z-\frac{bP_c}{RT_c}\right)+\frac{Pb_i}{RTZ-bP}-\frac{\Sigma_j x_j\sqrt{a_i a_j}}{d}\ln\left(\frac{Q+d}{Q-d}\right) \tag{A11}$$
$$+\frac{a(b_i+c_i)}{2(Q^2-d^2)}\left\{\ln\left(\frac{Q+d}{Q-d}\right)+\frac{2Qd}{Q^2-d^2}\right\}+\frac{8a}{d^3}\{c_i(3b+c)+b_i(3c+b)\}$$

where

$$Q=\frac{RTZ}{P}+\frac{b+c}{2} \tag{A12}$$

$$d=\sqrt{bc+\left(\frac{b+c}{2}\right)^2} \tag{A13}$$

The Patel-Teja EoS is expressed in the form of compressibility factor as follows:

$$Z^3+(C-1)Z^2+(A-2BC-B-C-B^2)Z+(BC+B^2C-AB)=0 \tag{A14}$$

where

$$A=\frac{aP}{(RT)^2} \tag{A15}$$

$$B=\frac{bP}{RT} \tag{A16}$$

$$C=\frac{cP}{RT} \tag{A17}$$

The Peng-Robinson equation of state [10] has the form:

$$P=\frac{RT}{v-b}-\frac{a_c\cdot\alpha(T)}{v(v+b)+b(v-b)} \tag{A18}$$

where v is the molar volume and R is the universal gas constant. The pure component parameters a_i and b_i are given by the following equations [10]:

$$a_c=0.457235\frac{R^2T_{ci}^2}{P_{ci}} \tag{A19}$$

$$\alpha(T)=\left[1+m_i\left(1-\sqrt{\frac{T}{T_{ci}}}\right)\right]^2 \tag{A20}$$

$$m_i=0.37464+1.5422\omega_i-0.26992\omega_i^2 \tag{A.21}$$

$$b_i=0.077796\frac{RT_{ci}}{P_{ci}} \tag{A.22}$$

$$a=a_c\cdot\alpha(T) \tag{A.23}$$

where ω_i, T_{ci} and P_{ci} are the acentric factor, critical temperature and critical pressure of component i. Also, the coefficients a and b for mixtures are calculated by Eqs. (2) and (3). The fugacity coefficient of the solvent in each phase is also obtained by [24]:

$$\ln\hat{\phi}_i=\frac{b_i}{b}(Z-1)-\ln(Z-B)+\frac{A}{2\sqrt{2}B}\left(\frac{2\Sigma_{j=1}^{N}y_j\sqrt{a_ia_j}(1-k_{ij})}{a}-\frac{b_i}{b}\right)\ln\left(\frac{z+(1-\sqrt{2})B}{z+(1+\sqrt{2})B}\right) \tag{A24}$$

where, A and B parameters are calculated by Eqs. (A15) and (A16).

The PR EoS is expressed in the form of compressibility factor as follows:

$$Z^3+(B-1)Z^2+(A-2B-3B^2)Z+(B^3+B^2-AB)=0 \tag{A25}$$

APPENDIX B

The group contribution method based on the modified Lydersen-Joback-Reid was used to estimate the critical pressure (P_c), critical temperature (T_c) and acentric factor (ω) of pure ILs. This method is summarized in the following four equations [11]:

$$P_c=\frac{M_w}{[C_M+\Sigma n\Delta P_M]^2} \tag{B1}$$

$$T_c=\frac{T_b}{A_M+B_M\Sigma n\Delta T_M-(\Sigma n\Delta T_M)^2} \tag{B2}$$

$$T_b=198.2+\Sigma n\Delta T_{bM} \tag{B3}$$

$$\omega=\log\left(\frac{P_c}{P_b}\right)\left[1+\frac{(T_b-43)(T_c-43)}{(T_c-T_b)(0.7T_c-43)}-\frac{(T_c-43)}{(T_c-T_b)}\right]-1 \tag{B4}$$

where, n is the number of times that a group appears in the molecule, ΔP_M is the modified contribution to the critical pressure, ΔT_M is the modified contribution to the critical temperature, ΔT_{bM} is the modified contribution to the normal boiling point (these parameters are dependent on the kind of groups that constitute the ILs and are given in Ref. [11]), and M_w is the molecular mass. The parameters that appear in Eqs. (B1) and (B2) were calculated as A_M=0.5703, B_M=1.0121, C_M=0.2573 and E_M=6.75. Moreover, T_b and T_c are in Kelvin and P_b is equal 1 atm.

APPENDIX C

C-1: Calculation of pure IL density:

In this example, the calculation of the density of [bmim][DCA] at T=363.15 K and P=101,325 Pa is shown by using the PR EoS.

Step 1: Physical properties of [bmim][DCA] (from Table 4):

T_c=954.5 K; $P_c=3.16\times10^6$ Pa; ω=0.8018;
M_W=0.20526 kg/mol; R=8.314 Pa·m^3/mol·K;

Step 2: Calculate parameters of the PR EoS (Eq. (A19)-(A23)):

a_c=9.1122 Pa·(m^3/mol)^2; $b=1.9537\times10^{-4}$ m^3/mol; m=1.4376;
$\alpha(T)$=2.4052; a=21.9171 Pa·(m^3/mol)^2;

Step 3: The two dimensionless parameters defined by Eqs. (A15) and (A16) are calculated as:

A=0.2436; B=0.0066;

Step 4: Obtain the following cubic equation for Z, Eq. (A25):

$$Z^3-0.9934Z^2+0.2304Z-0.0016=0$$

The above equation has three real roots, which the smallest positive root is acceptable:

Z=0.007;

Step 5: Calculate the pure IL density by the following equation:

$$\rho=\frac{PM_W}{RTZ}=990.7793\ \text{kg/m}^3$$

The experimental density [51] at T=363.15 K and P=101,325 Pa is 1,020.61 kg/m^3. By using the critical temperature, critical pressure and acentric factor that were given by Valderrama et al. [11,12], the mentioned liquid density is 711.2 kg/m^3.

C-2: Calculation of pure IL vapor pressure:

In this example, the calculation of the vapor pressure of [C_8mim][Tf_2N] at T=498.19 K is shown by using the PR EoS. At the saturation state, the fugacities of [C_8mim][Tf_2N] as vapor and liquid should be equal. For a pure compound the equality of fugacity reduces to the equality of fugacity coefficient.

$$\varphi^V=\varphi^L \tag{C1}$$

Hence, a pressure is assumed and the fugacities are calculated. The pressure is iterated until the two calculated fugacities become equal. The fugacity expression for pure compounds, based on PR EoS, results in:

$$\ln\varphi=(Z-1)-\ln(Z-B)+\frac{A}{2B\sqrt{2}}\ln\frac{Z+(1-\sqrt{2})B}{Z+(1+\sqrt{2})B} \tag{C2}$$

Step 1: Physical properties of [C_8mim][Tf_2N] (from Table 4):

T_c=1,187.8 K; $P_c=1.02\times10^6$ Pa; ω=0.9078;

Step 2: Calculate parameters of the PR EoS (Eq. (A19)-(A23)):

a_c=43.7167 Pa·(m^3/mol)^2; $b=7.5320\times10^{-4}$ m^3/mol; m=1.5522;
$\alpha(T)$=2.3931; a=104.6166 Pa·(m^3/mol)^2;

Step 3: To calculate the two dimensionless parameters of PR EoS defined by Eqs. (A15) and (A16), we need the value of vapor pres-

sure, so assuming a vapor pressure of 4.3612×10^{-2} Pa, using the Lee and Kessler correlation [24]:

$$\frac{P^{sat}}{P_c}=\exp(f_0+\omega f_1) \tag{C3}$$

where f_0 and f_1 are functions of the reduced temperature (T_r=T/T_c):

$$f_0=5.92714-\frac{6.09648}{T_r}-1.28862\ln T_r+0.16934(T_r)^6 \tag{C4}$$

$$f_0=15.2518-\frac{5.6875}{T_r}-13.4721\ln T_r+0.43577(T_r)^6 \tag{C5}$$

The two dimensionless parameters are calculated as:

$A=2.6595\times10^{-7}$; $B=7.931\times10^{-9}$;

Step 4: Obtain the following cubic equation for Z, Eq. (A25):

$$Z^3-0.998Z^2+2.5\times10^{-7}Z-2.04628\times10^{-15}=0$$

The above equation has three real roots. The smaller positive root is Z^L and the bigger positive root is Z^V:

$Z^L=8.469\times10^{-9}$; $Z^V=0.989$;

Step 5: Calculate the fugacity coefficient using the above two values of the compressibility factors:

$\varphi^V=0.999$; $\varphi^L=1.645$;

The comparison of the calculated fugacity coefficients indicates that the assumed pressure is close to the saturation pressure, but requires improvement. The next pressure is estimated as:

$$P_{(r+1)}=\left[P\frac{\varphi^L}{\varphi_V}\right]_r \tag{C.6}$$

where r is the iteration number. The solution is converged to fugacity coefficients values $\varphi^V=\varphi^L=0.989$ and vapor pressure P=0.0801 Pa. The experimental vapor pressure [54] at T=498.19 K is 0.1542 Pa. By using the critical temperature, critical pressure and acentric factor based on modified Lydersen-Joback-Reid method, the vapor pressure value is 2.296 Pa.

C-3: This example shows the bubble point calculation procedure for only one point of CO_2-[bmim][BF_4] binary mixture based on Patel-Teja EoS and genetic algorithm. The comprehensive block diagram of a computer program for bubble point calculation using genetic algorithm is shown in Fig. C1. Consequently, for bubble point calculation, where the liquid phase composition is known, the problem is to find the vapor composition, which can be calculated from set of *K*-value (Eq. (C7)) that satisfies Eq. (C8).

$$K_i=\frac{y_i}{x_i}=\frac{\hat{\varphi}_i^l}{\hat{\varphi}_i^v} \tag{C.7}$$

$$\Sigma_i K_i x_i=1 \tag{C.8}$$

Also, the pressure can be adjusted as:

$$P_{(r+1)}=P_r(\Sigma_i^N K_i x_i)_r \tag{C.9}$$

where r is the iteration number.

The procedure here is to do a bubble point calculation for each experimental data point. Fig. C1 indicates that for each calculation estimated values of P and y_1 are required to initiate iteration.

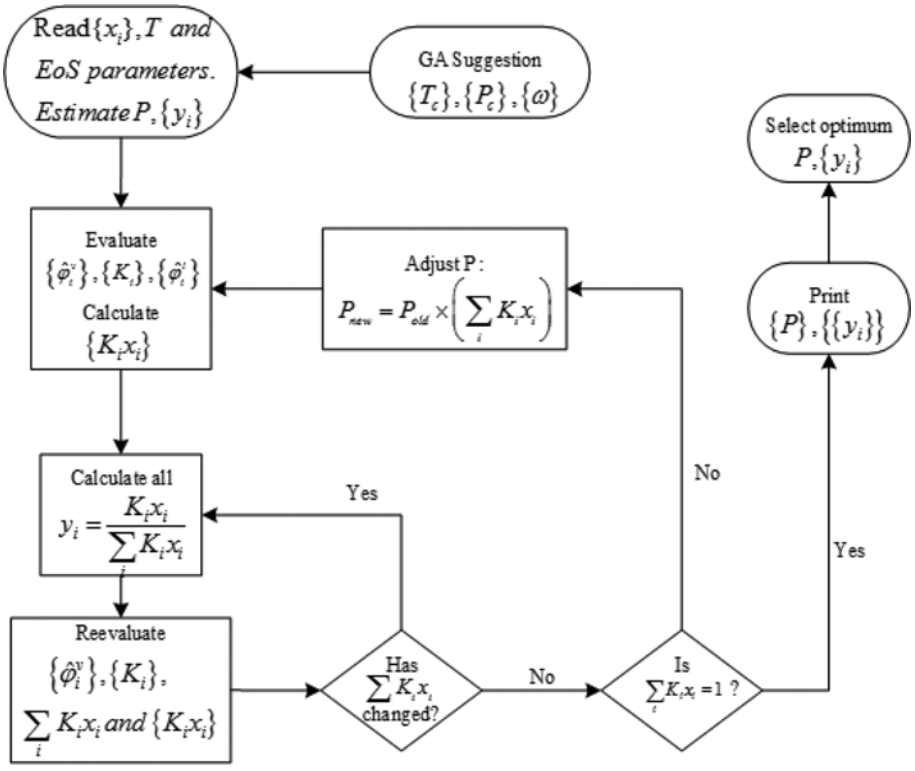

Fig. C1. Block diagram for bubble point pressure calculation.

Table C1. Initial values of T_c, P_c and ω for starting optimization process

Number	Component	T_c (K)	P_c (MPa)	ω
1	CO_2	304.2	7.39	0.2240
2	[bmim][BF_4]	632.3	2.04	0.8489

These estimations are here provided by the experimental data.

Step 1: The properties of component 1 (CO_2) and component 2 ([bmim][BF_4]) are read from Table 2.

The main aim of bubble point calculation is determination of T_c, P_c and ω of IL using GA. The GA needs a set of initial value of T_c, P_c and ω to start optimization process. Thus, the initial values of T_c, P_c and ω are provided from Ref. [11] (see Table C1).

Step 2: The PT EoS parameters for mixture components at T= 283.61 K and x_1=0.3035 (experimental value from Ref. [44]) are calculated and given in Table C2.

Step 3: The liquid mixture parameters a, b and c are calculated using the mixing rules namely, Eqs. (2)-(4), respectively. The binary interaction parameter between CO_2 and [bmim][BF_4] is assumed 0 (k_{ij}=0).

$a=34.1152\ \text{MPa}\cdot(\text{m}^3/\text{kmol})^2$ $b=131.039\times10^{-3}\ \text{m}^3/\text{kmol}$
$c=298.35\times10^{-3}\ \text{m}^3/\text{kmol}$

Step 4: A bubble point pressure of 1.5 MPa and the vapor compositions of y_1=0.3 and y_2=0.7 are assumed as the initial guess. The final result should not depend on the initial selected value. The PT EoS, Eq. (1), is set up for both phases. The dimensionless values of EoS parameters are calculated from Eqs. (A15)-(A17):

Liquid phase: $A=9.203$ $B=83.36\times10^{-3}$ $C=189.78\times10^{-3}$

The PT EoS in the form of liquid compressibility factor, is (see Eq. (A14)):

$$Z^3-810.2171\times10^{-3}Z^2+8.914Z-749.9976\times10^{-3}=0$$

The above equation has only one real root: $Z^L=84.9395\times10^{-3}$.

Vapor phase: $A=9.221$ $B=83.688\times10^{-3}$ $C=190.669\times10^{-3}$

The PT EoS in the form of the vapor compressibility factor, is (see Eq. (A14)):

$$Z^3-809.3306\times10^{-3}Z^2+8.908Z-754.4146\times10^{-3}=0$$

The above equation has only one real root: $Z^V=85.2809\times10^{-3}$.

Step 5: The calculated values of fugacity coefficients and equilibrium ratios are given in Table C3.

The value of $\Sigma K_i x_i$ is not equal to 1; consequently, the values of y_i and pressure must be reevaluated according to block diagram (see Fig. C1). These calculations show only one step for one bubble point pressure based on GA. The number of repetitions of this block diagram depends on the number of iterations and population of GA. As the procedure is performed for each generation of GA, the results are saved, and according to deviation of experimental data of P from the calculated value using GA was obtained (see (Eq. (5))). Then a new population of T_c, P_c, and ω is provided and a new set of errors according to objective function is expected. The procedure continues to obtain the best values of T_c, P_c, and ω for the minimum value of the objective function (see (Eq. (5))). At these conditions the optimized values of T_c, P_c, and ω are obtained. Moreover, there is a set of bubble point pressures for every generation of GA that corresponds to the best values of T_c, P_c, and ω. Finally, the solution converges; the optimized values of critical temperature, critical pressure and acentric factor together with their corresponding bubble point pressures are obtained.

Table C2. Calculated PT EoS parameters

	x_i	a_c MPa·(m³/kmol)²	m	α	$a=a_c\cdot\alpha$ MPa·(m³/kmol)²	b m³/kmol	c m³/kmol
Equation		A.2	A.3	A.4		A.5	A.6
Comp.1	0.3035	390.23×10^{-3}	730.97×10^{-3}	1.0510	410.12×10^{-3}	27.26×10^{-3}	20.99×10^{-3}
Comp.2	0.6965	6.6616	1.3511	2.0915	13.9330	176.26×10^{-3}	419.20×10^{-3}

Table C3. The calculated values of fugacity coefficients and *K*-values

	P (MPa)	x_i	y_i	$\hat{\varphi}_i^l$	$\hat{\varphi}_i^v$	K_i	$K_i x_i$
Equation				A.11	A.11	C.7	
Comp.1	1.5	0.3035	0.3	3.6919×10^{-3}	3.7441×10^{-3}	0.9859	0.2992
Comp.2	1.5	0.6965	0.7	2.5371×10^{-17}	2.2169×10^{-17}	1.1444	0.7971
Σ		1	1				1.0963